Chemical Engineering Journal 474 (2023) 145660

Contents lists available at ScienceDirect

Chemical Engineering Journal

journal homepage: www.elsevier.com/locate/cej

Shallow-bed reactor design for the autothermal oxidative dehydrogenation of ethane over $MoVTeNbO_x$ catalysts

Jiakang Chen, Praveen Bollini *, Vemuri Balakotaiah *

William A. Brookshire Department of Chemical & Biomolecular Engineering, University of Houston, Houston, TX 77204, USA

ARTICLE INFO

Keywords:
Cell model
Ignition and extinction
Eggshell catalyst
External mass transfer
Pore diffusion

ABSTRACT

We use a cell model with eggshell type catalyst particles to present a comprehensive ignition-extinction analysis of the oxidative dehydrogenation of ethane (ODHE) in autothermal operation. Our results reveal that external mass transfer could increase the ratio of ethane to oxygen on the catalyst surface, improving ethylene selectivity but decreasing ethane conversion. We show that ethylene selectivity is reduced, and a smaller region of multiplicity exists when diffusional limitations exist in the catalyst, which highlights the need for eggshell particles with a thin active layer. We also examine the impact of ethane to oxygen ratio, space time, catalyst particle size, and active layer thickness on the ignition and extinction behavior. A multi-layered bed with eggshell catalyst particles is proposed to optimize oxygen conversion and ethylene selectivity. Our results indicate the possibility of autothermal operation of the ODHE process with much higher productivity compared to traditional multi-tubular reactors.

1. Introduction

The abundance of shale gas in the United States has led to a significant increase in the availability and affordability of ethane, which is a key feedstock for ethylene production [1,2]. Ethane is a byproduct of natural gas production (about 5–10%), and the development of shale gas extraction and processing technologies has made it easier and more cost-effective to extract ethane from natural gas liquids [3]. Recently, the oxidative dehydrogenation of ethane (ODHE) has gained attention as an alternative method for producing ethylene from ethane. Compared to endothermic steam cracking, oxidative dehydrogenation of ethane (ODHE) utilizes oxygen to convert ethane to ethylene as part of a more thermodynamically favorable, highly exothermic process that is less prone to coking [4]. M1 phase bulk mixed metal oxide catalysts have exhibited exceptional selectivity in converting ethane to ethylene compared to other ODHE catalysts such as supported vanadia [5,6] and bulk NiO [7–9], and its yield has been shown to meet industrial standards [10]. Further design and optimization of this mixed metal oxide catalyst can make the ODHE process more commercially feasible [11,12]. The results of earlier research [13] indicate that the autothermal operation of ODHE over M1 phase catalysts at high pressure can yield significantly higher productivity and comparable ethane conversion and ethylene selectivity to that of steam cracking, while emitting 20% less carbon dioxide. Additionally, earlier research revealed that the autothermal reactor has a significantly smaller size compared to the traditional multi-tubular reactor while maintaining similar catalyst performance.

Ignition and extinction behaviors are commonly observed in highly exothermic reactions such as HCN synthesis, oxidative coupling of methane (OCM), and ODHE, and have been studied extensively by researchers. The observation of ignition and extinction behaviors in highly exothermic reactions led to the exploration of autothermal operation for catalytic partial oxidation reactions. Autothermal operation (AO) involves no intentional heat addition during the reaction process except for reactor start-up, and there is also no heat removal from the reactor [14]. Instead, heat is primarily removed by convection using a cold feed. Dietz et al. [15] conducted the synthesis of HCN over a Pt-Rh gauze catalyst in a bench-scale autothermal reactor and provided a detailed description of the autothermal operation procedure. Sarsani et al. [16] reported the observation of ignition and extinction behaviors in a lab-scale reactor during oxidative coupling of methane (OCM) using active La-Ce catalyst and reactants fed at ambient temperature. Sun et al. [17] investigated the feasibility of an autothermal reactor for the oxidative coupling of methane and demonstrated that C2 selectivity up to 80% can be achieved at methane conversions up to 20%. In previous work, we employed a 1D pseudo-homogeneous model to investigate the impact of feed ratio, space time, bed length, and pressure on ignition and

* Corresponding authors.
E-mail addresses: ppbollini@uh.edu (P. Bollini), bala@uh.edu (V. Balakotaiah).

https://doi.org/10.1016/j.cej.2023.145660
Received 4 May 2023; Received in revised form 10 August 2023; Accepted 24 August 2023
Available online 25 August 2023

Nomenclature

Roman letters

a_v	heat (mass) transfer area per unit bed volume, m^{-1}
C_{pv}	volumetric heat capacity of the reaction mixture, J/(m^3*K)
d_p	catalyst particle size, m
$D_{m,j}$	mass diffusivity of species j, m^2/s
$D_{eff,j}$	effective mass diffusion coefficient of species j, m^2/s
h	heat transfer coefficient, J/(s*m^3*K)
$\Delta H_{r,i}$	reaction enthalpy for reaction i, kJ/mol
$k_{c,j}$	mass transfer coefficient of species j, m/s
k_f	thermal conductivity, W/(m*K)
$r_{g,i}$	reaction rate i in the gas phase, s^{-1}
R_Ω	hydraulic radius, m
S_x	external surface area of the particle, m^2
T_f	fluid temperature,*K*
T_f^{in}	inlet fluid temperature,*K*
T_s	solid temperature,*K*
ΔT_{ad}	adiabatic temperature rise, K
u	linear velocity, m/s
V_c	volume of the active catalyst, m^3
$y_{f,j}$	mole fraction of species j in the fluid phase
$y_{f,j}^{in}$	inlet mole fraction of species j
$y_{s,j}$	mole fraction of species j in the solid phase

Greek letters

α_f	thermal diffusivity of the fluid, m^2/s
ν_{ij}	stoichiometric coefficient of species j for reaction i
ϵ_b	void fraction of the catalyst bed
$\tau_{mi,j}$	characteristic interphase mass transfer time of species j, s
τ_{hi}	characteristic interphase heat transfer time, s
τ_{ip}	characteristic intra-particle transfer time, s
τ	space time,*s*
ν_f	kinematic viscosity, m^2/s
ξ_c	depth of the active catalyst layer, m
ξ	dimensionless position within the active layer

extinction behavior. While the pseudo-homogeneous model used provided guidance for autothermal reactor design, it is important to note that the pressure drop can be significant for small catalyst particle sizes (<0.5 mm) required to reach the pseudo-homogeneous limit. Inter and intra-particle concentration and temperature gradients may not be neglected for finite size (≥1 mm) catalyst pellets used in commercial scale processes.

The main goal of this work is to determine the impact of internal and external transport effects on the ignition and extinction behavior of the ODHE reactor and to identify potential reactor designs that can be used for process scale-up. This manuscript is organized as follows: the next section presents both the mathematical and kinetic models, which take into account dehydrogenation, deep oxidation, secondary oxidation, and CO oxidation reactions. The kinetic model used has been validated in a previous publication using a series of differential and integral measurements [18]. In section 3, we present results on the impact of catalyst particle size, active layer thickness, ethane to oxygen ratio, space time, effective diffusivity in the pores, and pressure, on the region of multiplicity in a single eggshell catalyst particle. Section 4 examines the effects of packing strategies in multi-layered beds for two scenarios: (1) a fixed catalyst particle size with varying numbers of layers, and (2) a fixed space time with varying particle sizes. Increasing the number of layers with a fixed catalyst particle size barely changes the extinction point but can help achieve nearly 100% oxygen conversion as well as increase productivity. In another case, employing four layers of smaller catalyst particles can both reduce internal and external gradients and ultimately achieve complete conversion of oxygen. Finally, we summarize our results and identify limitations of our model as well as potential improvements that can be made through future research.

2. Model development

2.1. Cell model

Our prior work studied the ignition and extinction behaviors in the pseudo-homogeneous limit where the catalyst particle is sufficiently small (≤0.2 mm for the typical ODHE case). Balakotaiah et al. [14] stated that ignition and extinction could occur at the particle level when the adiabatic temperature is sufficiently high and catalyst particle size is large enough. Moreover, when all particles in a packed bed reactor are ignited, the reactor will operate either in the external mass transfer-controlled regime or a combined regime of pore diffusion and external mass transfer. This regime may be advantageous in some applications (such as OCM and ODHE) as it results in the maximum conversion of the limiting reactant for a given pressure drop. The primary mechanism for the existence of multiple steady states at the particle level is the inter-phase and intra-phase temperature gradients and is different from and independent of that at the reactor scale with heat and mass dispersion (or backmixing). Sun et al. discussed the impact of inter and intra-particle transport on the region of multiplicity for the OCM reaction system [17]. Unlike these reaction systems, to the best of our knowledge, there has been no prior work on analyzing the impact of inter and intra-particle gradients on the autothermal operation range, ethane conversion, and ethylene selectivity for the ODHE process.

Multi-layered beds with finite-size eggshell catalyst particles may be used to reduce pressure drop and reach full conversion of the limiting reactant as shown in Fig. 1a. In an eggshell catalyst particle, the outer layer is coated with active M1 phase catalyst, while the inner core consists of inert materials such as SiC or α-Al_2O_3 (see Fig. 1b). This design allows for particle level ignition while avoiding pore diffusional effects that may be detrimental to product conversion and selectivity. The specific kinetics of ODHE indicate that the oxygen order of the main dehydrogenation reaction is lower than that of the side reactions under most operating conditions, suggesting that lower oxygen concentrations favor ethylene selectivity. As illustrated in Fig. 3a, this kinetic feature can be exploited to increase the ethane to oxygen ratio (lowering oxygen mole fraction) on the catalyst surface via external mass transfer.

Froment et al. [19] discussed several reactor models to simulate the inter-phase temperature and concentration gradients and intra-particle diffusional effects. Here, a cell model is well suited to investigate the impact of inter-phase mass and heat transfer resistance (fluid to catalyst surface) and intra-particle concentration (within the particle) on the ignition and extinction behavior. In this cell model, the computations are simplified by not considering heat conduction (or backflow) through the catalyst bed. A more detailed and continuous model would require consideration of a significantly complex model, making the computation much more difficult. Balakotaiah et al. [20] have pointed out that inclusion of bed scale heat backflow could move the extinction point to a slightly lower feed temperature and lead to the elimination of certain intermediate states. While the location of the extinction point may be affected by bed-scale heat backflow, the cell model used in this study is sufficient to examine ignition and extinction behavior as well as the feasibility of scale-up. The validity of the cell model when particle level multiplicity exists and comparison of its predictions to experimentally observed temperature patterns has been discussed in recent publications [21,22].

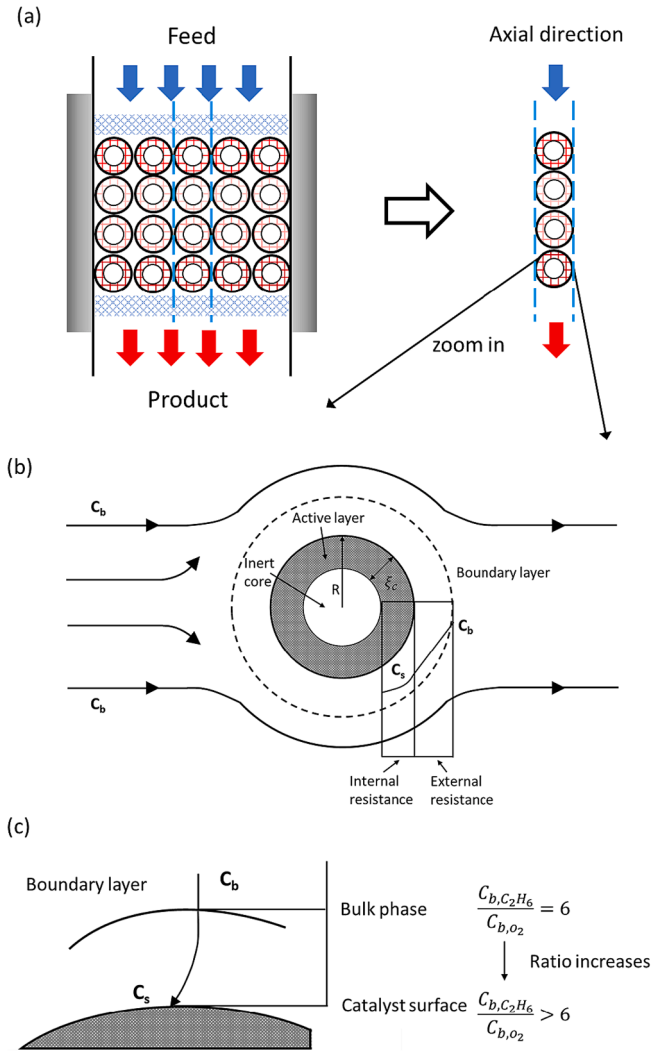

Fig. 1. Schematic diagram of (a) multi-layered bed with eggshell particles (b) single eggshell catalyst particle (c) boundary layer around the catalyst surface.

The steady-state species and energy balances of the cell model in the fluid phase are given by:

$$y_{f,j}^{in} - y_{f,j} + \frac{\tau}{\tau_{mi,j}}(1-\epsilon_b)\left(y_{s,j} - y_{f,j}\right) + \tau\epsilon_b \sum_{i=1}^{N} \upsilon_{ij} r_{g,i}\left(\overline{y}_f, T_f\right) = 0; \quad (1)$$

$$T_f^{in} - T_f + \frac{\tau}{\tau_{hi}}(1-\epsilon_b)\left(T_s - T_f\right) + \tau\epsilon_b \sum_{i=1}^{N} \frac{\left(-\Delta H_{r,i}\right) r_{g,i}\left(\overline{y}_f, T_f\right)}{C_{pv}} = 0; \quad (2)$$

where τ is the space time, $y_{f,j}$ is the mole fraction of species j in the fluid phase, $y_{s,j}$ is the mole fraction of species j on the catalyst surface, ϵ_b is the void fraction of the catalyst bed, υ_{ij} is the stoichiometric coefficient of species j in reaction i, $r_{g,i}\left(\overline{y}_f, T_f\right)$ is the rate of reaction i having unit of s^{-1} in the fluid phase, further details and explanation can be found in the Supplementary Information. T_f is the fluid phase temperature, T_s is the catalyst surface temperature, $-\Delta H_{r,i}$ is the reaction enthalpy at fluid phase temperature, C_{pv} is the volumetric heat capacity of the reaction mixture in the fluid phase. The inter-phase heat and mass transfer times can be expressed as follows:

$$\tau_{mi,j} = \frac{1}{k_{c,j} a_v}, \quad (3)$$

$$\tau_{hi} = \frac{C_{pv}}{h a_v}, \quad (4)$$

$$a_v = \frac{6}{d_p}, \quad (5)$$

where $k_{c,j}$ is the gas to solid mass transfer coefficient of species j, h is the heat transfer coefficient and a_v is the heat (mass) transfer area per unit bed volume. Typical inter-phase mass ($\tau_{mi,j}$) and heat transfer times (τ_{hi}) at the operating temperature range between 10 and 50 ms for a 4 mm catalyst particle. The heat and mass transfer coefficients are dependent on temperature and velocity as shown below [23,24]:

$$\frac{k_{c,j} d_p}{D_{m,j}} = 2 + 1.1\left(\frac{d_p u}{\nu_f}\right)^{0.6}\left(\frac{\nu_f}{D_{m,j}}\right)^{1/3}; \quad (6)$$

$$\frac{h d_p}{k_f} = 2 + 1.1\left(\frac{d_p u}{\nu_f}\right)^{0.6}\left(\frac{\nu_f}{\alpha_f}\right)^{1/3}; \quad (7)$$

where d_p is catalyst particle diameter, $D_{m,j}$ is the bulk mass diffusivity of species j which is calculated by Fuller equation [25], u is the linear velocity, ν_f is the kinematic viscosity, k_f is the thermal conductivity and α_f is the thermal diffusivity of the fluid phase. [Remark: In the present study, the reaction/source terms in Eqs. (1) and (2) are set to zero as there are no homogeneous reactions].

The steady-state species and energy balances of the cell model in the catalyst phase are described below:

$$\frac{D_{eff,j}}{r_p^2}\left(\frac{d^2 y_{s,j}}{d\xi^2} + \frac{2}{\xi}\frac{dy_{s,j}}{d\xi}\right) + \sum_{i=1}^{N} \upsilon_{ij} r_{s,i}\left(\overline{y}_s, T_s\right) = 0; \quad (8)$$

$$\frac{T_f - T_s}{\tau_{hi}} + \sum_{i=1}^{N} \frac{\left(-\Delta H_{r,i}\right) < r_{s,i}\left(\overline{y}_s, T_s\right)>}{C_{pv}} = 0; \quad (9)$$

with the boundary conditions:

$$\frac{dy_{s,j}}{d\xi} = 0, at\ \ \xi = \left(d_p - 2\xi_c\right) \Big/ d_p; \quad (10)$$

$$\frac{dy_{s,j}}{d\xi} = \frac{r_p k_{c,j}}{D_{eff,j}}\left(y_{f,j} - y_{s,j}\right), at \xi = 1; \quad (11)$$

where $D_{eff,j}$ is the effective mass diffusivity in the catalyst pores of the species j, ξ_c is the depth of the active catalyst layer, ξ is the dimensionless position along the active layer which ranges from $(d_p - 2\xi_c)/d_p$ to 1. Here, the quantity $< r_{s,i}\left(\overline{y}_s, T_s\right)>$ is the volumetric averaged reaction rate calculated as shown below:

$$< r_{s,i}\left(\overline{y}_s, T_s\right)> = \frac{\int_{(d_p-2\xi_c)/d_p}^{1} r_{s,i}\left(\overline{y}_s, T_s\right)\xi^2 d\xi}{\int_{(d_p-2\xi_c)/d_p}^{1} \xi^2 d\xi}; \quad (12)$$

The pseudo-arc-length continuation method was used to numerically compute the steady-state bifurcation diagrams of this model through Python and Matlab. The number of mesh points used to describe gradients in the catalyst layer ranged from 25 to 100 for the eggshell catalyst particles, and the number of mesh points was adjusted until no further changes were detected in the computational results.

As shown in the Supplementary Information, the pressure drop through a shallow-bed of few particle layers at typical operating conditions is found to be of the order of 0.003 kPa, which is very small. Hence, the pressure drop is neglected in the calculations using the cell model.

2.2. ODHE kinetic model

In our prior work we proposed a global kinetic model for ODHE

catalysis over an $MoVTeNbO_x$ catalyst that was validated using a wide range of differential and integral data [18]. The reaction network is comprised of six catalytic reactions without any homogeneous reactions, as listed below:

Step 1 $C_2H_6 + 0.5O_2 \rightarrow C_2H_4 + H_2O$, $\Delta H^0_{r,1} = -105 kJ/mol$

Step 2 $C_2H_6 + 2.5O_2 \rightarrow 2CO + 3H_2O$, $\Delta H^0_{r,2} = -863 kJ/mol$

Step 3 $C_2H_6 + 3.5O_2 \rightarrow 2CO_2 + 3H_2O$, $\Delta H^0_{r,3} = -1428 kJ/mol$

Step 4 $C_2H_4 + 2O_2 \rightarrow 2CO + 2H_2O$, $\Delta H^0_{r,4} = -757 kJ/mol$

Step 5 $C_2H_4 + 3O_2 \rightarrow 2CO_2 + 2H_2O$, $\Delta H^0_{r,5} = -1323 kJ/mol$

Step 6 $CO + 0.5O_2 \rightarrow CO_2$, $\Delta H^0_{r,6} = -283 kJ/mol$

It is important to note that the 6 oxidation reactions under consideration are highly exothermic, and their adiabatic temperature rise values have been calculated previously by Chen et al. [13] for various inlet temperatures and feed ratios. For instance, the adiabatic temperature rise for the main dehydrogenation reaction (step 1) at an inlet temperature of 310 K, ethane to oxygen ratio of 6, and pressure of 1 bar is 398 K. This corresponds to a maximum per pass ethane conversion of 33%. Thus, it is challenging to effectively remove the heat and maintain isothermal conditions in a multi-tubular reactor for this highly exothermic reaction system without dilution of feed and acceptable per pass ethane conversions. Instead, autothermal operation takes advantage of the high adiabatic temperature rise to achieve high productivity, as well as desirable ethane conversion and ethylene selectivity. The rate expression and kinetic parameters can be found in sections S1 and S2 of the Supplementary Information, respectively. The key features of the kinetic model have already been discussed in our previous work and will be reviewed in detail in later sections.

3. Steady-state bifurcation analysis of single catalyst particle

In our recent work, we studied the impact of different design and operating conditions (space time, bed length, operating pressure and so forth) on ignition and extinction behavior using the pseudo-homogeneous model, while neglecting the impacts of external and internal gradients. In this section, we present a comprehensive bifurcation analysis of a single eggshell catalyst particle (or a catalyst bed consisting of a single layer) and determine the impact of catalyst particle size, space time, and pore diffusion on the region of autothermal operation. We present all calculations for P = 1 bar and adiabatic conditions. Additional results demonstrating the effects of various parameters such as the thickness of the active layer, ethane to oxygen feed ratio, operating pressure, and feed dilution are available in the Supplementary Information.

3.1. Impact of external mass and heat transfer

Before discussing the cell model, we examine the inter-phase mass and heat transfer times (see section S3 of Supplementary Information for details). The inter-phase mass and heat transfer times range from the order of 1 ms to the order of 100 ms for various feed temperatures and catalyst particle sizes. The results reveal that the inter-phase mass and heat transfer times decrease as the feed temperature increases, and almost quadratically with increasing catalyst particle size. Fig. 2 shows a bifurcation diagram of exit fluid and particle temperature as a function of feed temperature for different catalyst particles with a feed ratio of 6 and a space time of 0.4 s, and an active layer thickness equal to 0.1 times the particle diameter. For a catalyst particle size of 1 mm, the inter-phase mass and heat transfer times are two orders of magnitude lower than typical operating space time of (100–800 ms). Therefore, the pseudo-homogeneous limit can be reached for the energy balance if the catalyst particle size is smaller than 1 mm, and ignition and extinction occur at the reactor level due to bed scale heat dispersion. This observation can help explain why the exit fluid temperature is almost identical to the exit particle temperature for the 1 mm catalyst particle as

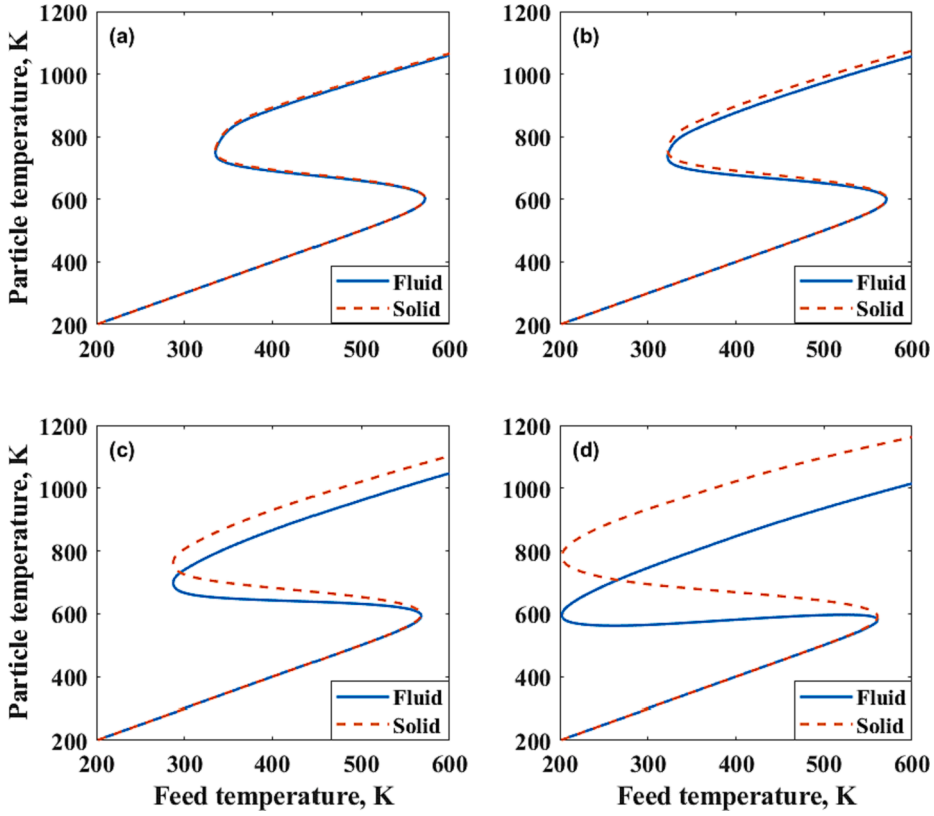

Fig. 2. Computed bifurcation diagrams of exit temperature versus feed temperature for (a) 1 mm particle (b) 2 mm particle (c) 4 mm particle (d) 8 mm particle. Reaction conditions: P = 1 bar, $C_2H_6 : O_2 = 6$, $\tau = 0.4$ s, $\xi_c = 0.1\ d_p$.

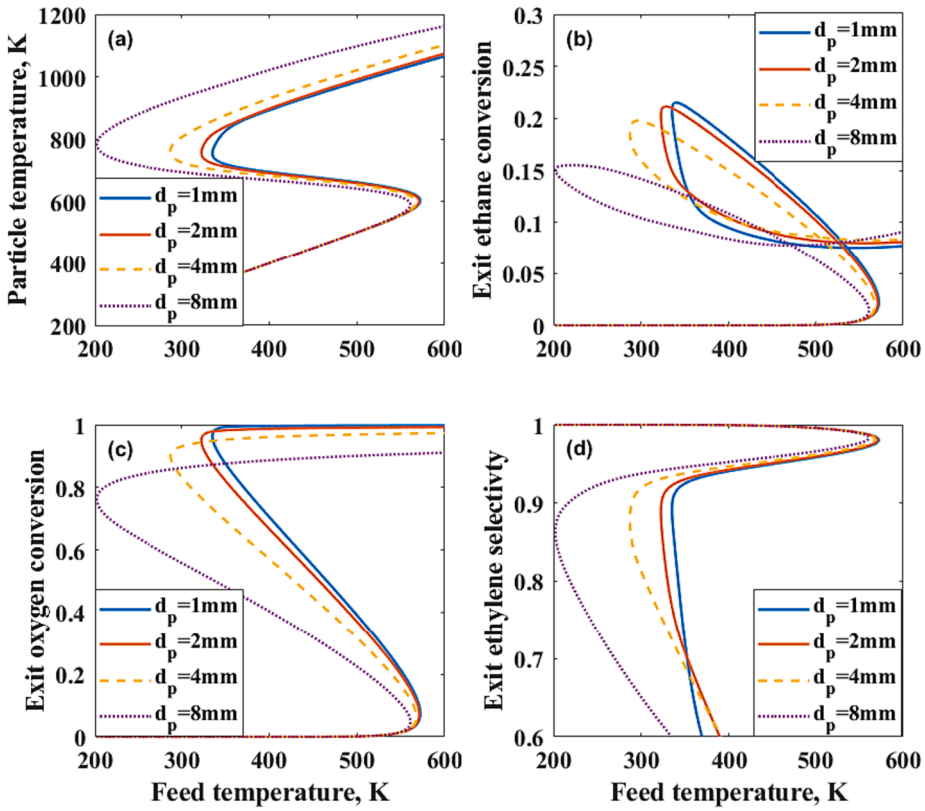

Fig. 3. Computed bifurcation diagrams of exit (a) particle temperature (b) ethane conversion (c) oxygen conversion (d) ethylene selectivity versus feed temperature. Reaction conditions: P = 1 bar, $C_2H_6 : O_2 = 6$, $\tau = 0.4$ s, $\xi_c = 0.1\ d_p$.

shown in the Fig. 2a. At a temperature of 650 K, the inter-phase heat transfer time for a catalyst particle 8 mm in diameter is 81 ms, which is comparable to the operating space time. It is found that the ignition point moves to higher feed temperature and the extinction point moves to lower feed temperature as the particle size increases, leading to larger regions of multiplicity. Moreover, the temperature difference between the fluid and particle phases also increases with increasing particle size. It is interesting to note that the particle temperature at the extinction point increases from 730 K to about 785 K as particle size increases from 1 mm to 8 mm.

The impact of particle size on catalyst particle temperature, exit ethane and oxygen conversion, and exit ethylene selectivity with fixed space time is shown in the Fig. 3. The results show that fluid phase ethane and oxygen conversions decrease with particle size due to stronger inter-phase mass transfer resistance as shown in Fig. 3b and c. For the specific ODHE kinetics under consideration, the activation energy of the main dehydrogenation reaction is only 89.4 kJ/mol, significantly lower than that of the side reactions, suggesting that the rates of side reactions can be expected to increase more sensitively with temperature than the main dehydrogenation reaction. Higher operating temperatures therefore result in reduced selectivities by favoring side reactions. Besides, the oxygen dependency of the main dehydrogenation reaction varies between zero and first order depending on the oxygen mole fraction. For example, the dehydrogenation reaction exhibits zeroth order dependency on oxygen partial pressure when the oxygen mole fraction is not very low (above 0.01) and shifts towards first order dependency on oxygen partial pressure as the oxygen mole fraction decreases further. Therefore, we can increase the ethylene selectivity by keeping the oxygen mole fraction low, as side reactions have a higher oxygen order under these conditions. Since oxygen is the limiting reactant, the ethane to oxygen ratio at the catalyst surface is higher than that in the fluid phase when the particle is in the external mass transfer-controlled regime. Higher ethane to oxygen feed ratios (low oxygen mole fractions) have a favorable effect on ethylene selectivity. However, it is found that the ethylene selectivity decreases from 89% to 87% as the particle diameter increases from 1 mm to 8 mm as shown in Fig. 3d. This is because the higher particle temperatures in larger particles lead to lower ethylene selectivity despite the fact that these larger particles have stronger external mass transfer resistance.

Fig. 4 illustrates the oxygen mole fraction, and ethylene mole fraction at the extinction point within the active catalyst layer with a constant C_2H_6:O_2 feed ratio of 6 and space time of 0.4 s. In this plot, radial position 1 represents the dimensionless position at the catalyst surface and 0 represents the dimensionless position at the interface between the inert core and the active catalyst layer. The results indicate that oxygen is almost fully consumed within approximately 0.3 mm at the extinction point as it diffuses inside the active catalyst layer. Oxygen only exists in the outer 40% of the active layer in the case of an 8 mm particle, implying that the reaction zone's depth is only 8% of the particle radius, and about 20% of the particle volume is utilized for the reaction. After oxygen is fully consumed in the catalyst layer (the case of 8 mm particle), the ethylene mole fraction remains constant because no more reactions occur as shown in Fig. 4b. The oxygen mole fraction gradient is negligible for a particle diameter of 2 mm (and an active layer thickness of 0.2 mm), indicating that pore diffusional effects are not significant in this case. Also, the active layer depth of 0.2 mm should also be sufficient for particle ignition. To prevent pore diffusional limitations, we can design multi-layered beds of eggshell particles with a constant active layer thickness of 0.2 mm. As pore diffusional effects can negatively impact intermediate product selectivity, it may be advantageous to utilize an eggshell catalyst particle that has a fixed active layer depth and inert core for catalytic ODHE chemistry.

The impact of space time on particle ignition, reactants conversion and ethylene selectivity are illustrated in Fig. 5. As the space time increases from 0.2 to 1.2 s, the ignition and extinction points shift toward lower feed temperatures. The region of multiplicity shrinks slightly as

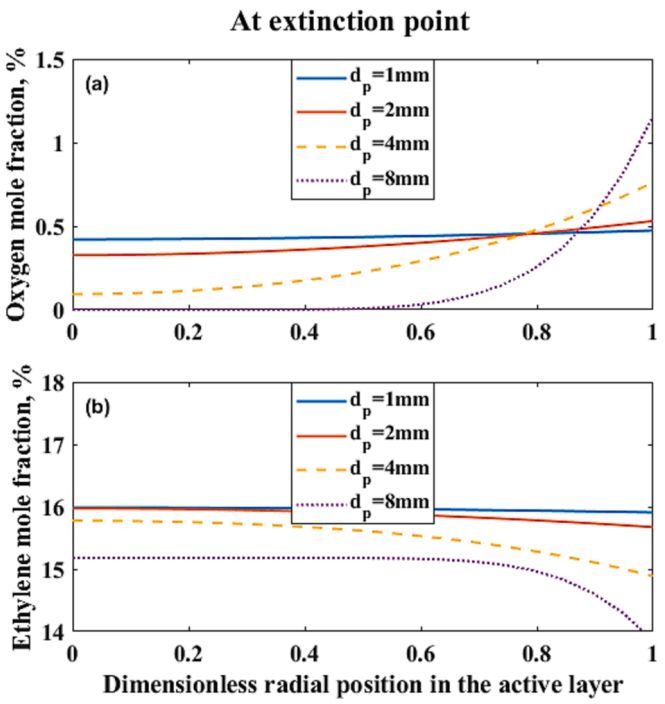

Fig. 4. Computed profiles of (a) oxygen mole fraction, and (b) ethylene mole fraction at the extinction point for eggshell catalyst particles of various sizes. Reaction conditions: P = 1 bar, $C_2H_6 : O_2 = 6$, τ=0.4 s, $\xi_c = 0.1\ d_p$.

space time increases due to pore diffusional limitations. This is due to the fact that the catalyst layer thickness in this case is 0.4 mm and is not optimal. It is also observed that the particle temperature on the ignited branch is lower at higher space time due to higher rates of heat removal. Fig. 5a shows that the exit particle temperature decreases with increasing space time, which favors the main dehydrogenation reactions. Since the main dehydrogenation reaction consumes more ethane per mole of oxygen compared with the side reactions, higher space times lead to higher ethane conversion. For the same reason, ethylene selectivity increases as space time increases. These results suggest that it is feasible to achieve approximately 88% ethylene selectivity at 20% ethane and 90% oxygen conversion using a single layer of 4 mm diameter eggshell catalyst particles with an active layer thickness of 0.4 mm. We choose an ethane to oxygen feed ratio of 6 because it enables autothermal operation close to the extinction point with an ambient temperature feed as shown in Fig. S1. Feed ratios higher than 6 yield higher ethylene selectivities at the expense of lower ethane conversions. Although complete oxygen conversion and higher ethylene selectivities can be achieved by increasing the space time from 0.2 s to 1.2 s, reactor productivities are significantly lower at these higher space times. [Remark: the cell model will approach the pseudo-homogenous model as space time increases.] Therefore, an optimum set of reaction conditions will exist at which both high catalyst performance and high productivity are simultaneously achieved.

3.2. Impact of pore diffusion

Intra-particle diffusion or mass transfer time within the catalyst is calculated using the following equations:

$$\tau_{ip} = \frac{R_\Omega^2}{D_{eff}}, \tag{13}$$

$$R_\Omega = \frac{V_c}{S_x}, \tag{14}$$

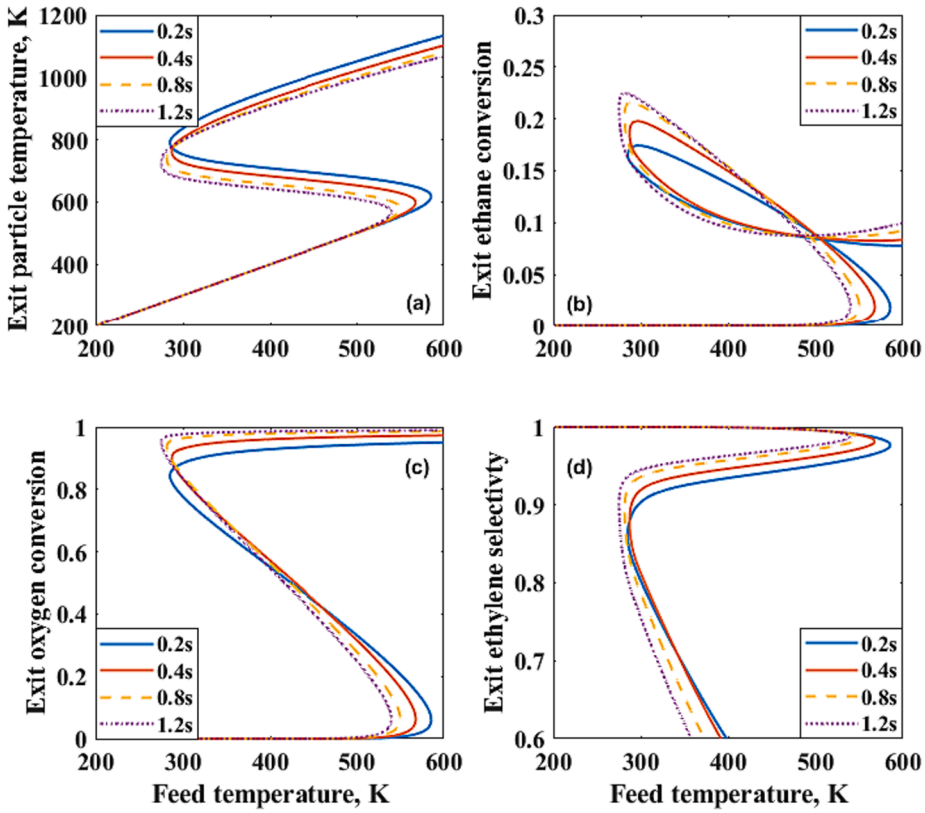

Fig. 5. Computed bifurcation diagrams of exit (a) particle temperature, (b) ethane conversion, (c) oxygen conversion, and (d) ethylene selectivity versus feed temperature at different space times. Reaction conditions: P = 1 bar, $C_2H_6 : O_2 = 6$, $d_p = 4$ mm, $\xi_c = 0.1\ d_p$.

where τ_{ip} is the intra-particle diffusion or mass transfer time, R_Ω is the hydraulic radius (or effective diffusion length), V_c is the volume of the active catalyst, S_x is the external surface area of the particle, D_{eff} is the effective diffusivity of the limiting reactant (oxygen here) inside the catalyst pore. Table 1 shows the calculated characteristic intra-particle (catalyst layer) diffusion times with different effective pore diffusivity values for full and eggshell catalyst particles at a temperature of 750 K. The results show that intra-particle diffusion time increases quadratically with particle diameter for fully active particles while the intra-particle diffusion time of the eggshell particles increases at a slower rate due to the active layer thickness remaining unchanged. When the effective diffusivity is one hundredth of the bulk mass diffusivity, the intra-particle diffusion time scale for a 4 mm particle is 111 ms, comparable to typical operating space times. Intra-particle diffusion can therefore have a determinative impact on ignition and extinction behavior at time scales comparable to the space time. Fig. 6 shows the impact of pore diffusion on the region of multiplicity using different effective pore diffusivity values. Generally speaking, the effective pore diffusivity of the species in porous catalyst depends on the pore size, pore-size distribution, pore-blockage, and tortuosity [26]. Sadakane et al. [27] utilized the seven-membered ring channel model with a diameter of 0.35 nm to calculate the theoretical pore volume in M1 catalyst, which was found to be approximately 0.018 cm^3/g. Nguyen et al. [28] pointed out that the pore volume of $MoVTeNbO_x$ ranges from 0.4 to 3.1 cm^3/g and its BET surface area ranges from 4.6 to 37.9 m^2/g. Annamalai et al. [29] reported a pore volume of $7.9*10^{-4}$ cm^3/s, which is one order of magnitude smaller than the theoretical values discussed above. These low pore volumes may result from metal cations such as Te blocking heptagonal pores, a phenomenon that has previously been proposed to stabilize C-H bond activation transition states [30]. Such lower than expected pore volumes and pore blocking effects render it challenging for us to accurately estimate effective pore diffusivity values. Here, we assume the pore diffusivity is a constant fraction of the bulk diffusivity and change this factor from unity to 0.01 as shown in the Fig. 6. As can be expected, the region of multiplicity shrinks as the pore diffusivity decreases. In addition, reactants conversion and ethylene selectivity decrease with stronger pore diffusion limitation. These results show that designing eggshell catalyst particles with a fixed active layer depth can help avoid pore diffusional effects, thereby aiding in scale-up analysis of the ODHE process.

3.3. Impact of pressure effects

This section discusses the impact of pressure effects for two scenarios: fixed linear velocity and fixed mass velocity. In the case of fixed linear velocity, the space time remains constant, while the mass velocity increases with increasing total pressure. In the case of fixed mass velocity, the space time increases with increasing total pressure. In both cases, reaction rates are proportional to total pressure.

Fig. S3 illustrates the impact of total pressure on the region of multiplicity with fixed linear velocity at an ethane to oxygen feed ratio of 6, a particle diameter of 1 mm, and a space time of 0.4 s. High pressure calculations employ a 1 mm particle with a 0.05 mm active layer instead of a 4 mm particle with a 0.2 mm active layer used in the previous section because effective pore diffusivity is inversely proportional to total pressure. Using smaller particles with shorter active layers can help circumvent pore diffusional effects that typically shrink the region of multiplicity and reduce ethylene selectivity. The study found that the extinction point shifts to a lower feed temperature while the ignition point remains the same, resulting in an expanded region of multiplicity. Two factors may explain this outcome. Firstly, as total pressure increases from 1 to 5 bar, external and mass transfer times increase roughly 3–4 times as shown in Table S3. Stronger external mass and heat transfer lead to an expansion of the region of multiplicity. Secondly, side reactions in the ODHE kinetic model carry a higher pressure dependency than the main dehydrogenation reaction, implying that highly exothermic side reactions are more predominant and generate more heat as total pressure increases, thereby expanding the region of multiplicity. The disproportionate effect of total pressure on the rates of side reactions can also help account for the observed decrease in ethylene selectivity as the total pressure increases from 1 to 5 bar.

In contrast to the case where the linear velocity is fixed, if the mass velocity remains unchanged, space time will increase as the total pressure increases. However, the productivity does not vary with increasing total pressure under this condition. Fig. S4 shows the impact of total pressure with fixed mass velocity on exit particle temperature, reactants conversion, and ethylene selectivity. The space time changes from 0.4 to 2.0 s as the total pressure increases from 1 to 5 bar. Compared to the case where the linear velocity is kept fixed, it is found that the extinction point moves to much lower feed temperatures as the total pressure is increased because higher space times expand the region of multiplicity, as shown in Fig. 5. A lower feed temperature at the extinction point corresponds to a lower operating temperature, which in turn favors the main dehydrogenation reaction. Hence, we find that it is feasible to attain an ethane conversion of approximately 18% and an ethylene selectivity of 86% by operating at a total pressure of 5 bar over a 1 mm eggshell catalyst particle at a space time of 2 s.

Lastly, we would like to briefly discuss the impact of dilution on autothermal reactor operation. In traditional steam cracking processes a large amount of steam is used as diluent to decrease the hydrocarbon partial pressure [31]. Multi-tubular reactors also use significant unreactive dilutants such as helium or nitrogen to lower adiabatic temperature rise values and reaction rates [32,33]. Fig. S5 shows the particle temperature, reactants conversion and ethylene selectivity versus feed temperature with 50% methane dilution. The adiabatic temperature rise for these reaction conditions is about 360 K. Methane is not reactive over the M1 phase catalyst and serves as an effective absorber of heat. A space time of 3 s was chosen to move the extinction point closer to ambient temperature. We observe that a shallow bed with eggshell particles is a feasible autothermal reactor design that could achieve about 95% ethylene selectivity at about 37% ethane conversion under 50% methane dilution.

Table 1
The intra-particle mass and heat transfer times were calculated for two types of catalyst particles (full or eggshell) using different effective pore diffusivities. The active layer length of the eggshell is 0.4 mm, operating temperature is 750 K.

Temperature (K)	Particle size (mm)	τ_{ip}, full (ms)	τ_{ip}, eggshell (ms)
$D_{eff} = \frac{D_m}{10}$	1	2.9	2.87
	2	11.7	7.2
	4	46.7	11.1
	8	187	13.7
$D_{eff} = \frac{D_m}{100}$	1	29	28.7
	2	117	72
	4	467	111
	8	1870	137

4. Analysis of multi-layered beds with eggshell particles

As mentioned earlier, a primary goal of this work is to evaluate the impact of external and internal transport effects on the ignition and extinction behavior of the ODHE system, and to explore the feasibility of conducting these reactions using eggshell catalyst particles. While the single layer calculations discussed in the previous section are useful in understanding transport effects, they lead to only limited reactant conversions, and hence are not practical. Sun et al. [17] reported fluid phase oxygen conversions for the OCM process that reached almost 100%, and C2 product selectivities that were improved slightly when using multi-layered beds. In this section, we consider the more realistic case of a multi-layered but shallow catalyst bed with eggshell particles to increase reactant conversion with two packing strategies: a) fixed particle size with varying space time and number of layers, and b) fixed space time

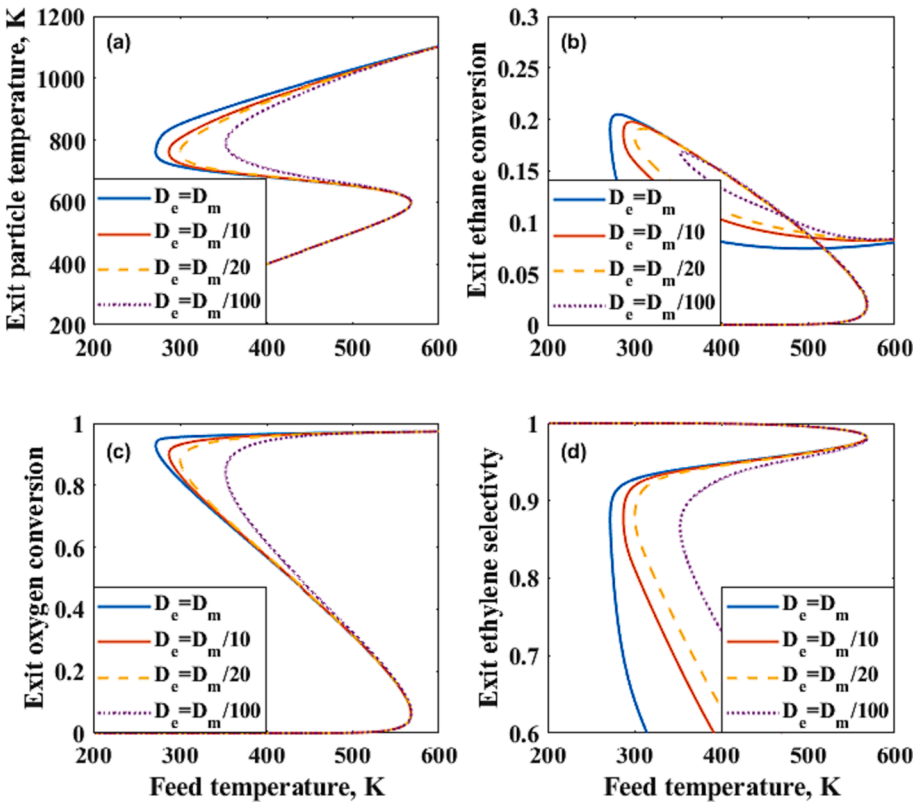

Fig. 6. Bifurcation diagram discussing the impact of pore diffusion. Reaction conditions: P = 1 bar, $C_2H_6 : O_2 = 6$, $d_p = 4$ mm, $\xi_c = 0.1\ d_p$, $\tau = 0.4$ s.

with varying particle diameter and number of layers. Reactor productivity is an important factor in scale-up analysis, and it is inversely proportional to the space time. In the first scenario, maintaining a constant catalyst particle size while increasing the number of layers may enhance oxygen conversion, but it may also decrease process productivity. On the other hand, fixing the space time can ensure consistent productivity, but using different catalyst particle sizes may also affect the feasibility of autothermal operation.

4.1. Fixed catalyst particle size with varying number of layers

Three cases of a fixed catalyst particle size with varying number of layers and space times are shown schematically in Fig. 7a. The particle diameter is selected to be 4 mm to facilitate external mass transfer and reduce the oxygen mole fraction at the particle surface (and catalyst layer) which favors ethylene production. The space time in each layer is chosen to be 0.2 s to achieve higher ethylene productivity and to ensure that the feed temperature of the extinction point is still close to ambient temperature. Fig. 8 shows ethane and oxygen conversions and ethylene selectivity for beds with varying number of layers of 4 mm sized particles containing a 0.2 mm active layer. Since the optimum operating point is typically 5–10 K higher than the extinction point, here we only show the ignited branch of the reactor (or exit value of the last cell) in the calculations. In this design, the active layer depth is limited to 0.2 mm due to the negative impact of pore diffusion, which not only decreases ethylene selectivity but also shrinks the region of autothermal operation. Our calculations reveal that the feed temperature at the extinction point remains almost unchanged with increasing number of the layers. This could be attributed to the constant particle size and the fact that most of the reaction takes place within the first layer. The results demonstrate that as the number of layers increases from 1 to 3, the exit oxygen conversion at the extinction point shows a significant increase from 87% to almost 100%, while the exit ethane conversion increases from 15.5% to 18%. We also note that the ethylene selectivity remains nearly unchanged as the number of layers increases.

Fig. 9 shows a plot of the solid and fluid temperatures in each layer corresponding to a feed temperature that is slightly to the right of the extinction point for a bed with three layers [A complete bifurcation diagram for this case is given in Fig. S6]. We note that the solid temperature is higher in the first layer and decreases in the flow direction. This is due to the fact that the Lewis number for this system is less than unity [34]. Table S3 lists characteristic inter-phase mass and heat transfer times with high ethane to oxygen ratio for different feed temperatures. From this table, it is observed that the inter-phase mass transfer time is slightly smaller than the inter-phase heat transfer time, which indicates that the Lewis number (thermal diffusivity of the gas mixture to the bulk diffusivity of the limiting reactant O_2) is about 0.8–0.9. When Lewis number is smaller than unity, the mass transfer rate is higher than the heat transfer rate, which can result in a solid temperature that exceeds the adiabatic temperature rise. Therefore, lower Lewis number could facilitate ethane conversion but mitigate ethylene selectivity. We also notice that the solid temperature decreases with increasing number of layers while the fluid temperature increases monotonically. Gundlapally et al. [35] also observed similar results, wherein the solid temperature decreases along the monolith channel with developing flow for after-treatment systems. We note that when heat conduction (back flow) is included, the variation in the temperature of the solid is smaller (or solid temperature profile becomes flatter) compared to that predicted by the cell model (though it is still monotonically decreasing).

4.2. Fixed space time with varying number of layers

When the space time is kept constant, the particle size could vary inversely with the number of layers, unlike the situation where the particle size remains constant. In order to have a better understanding on the impact of this packing strategy on the ignition and extinction behavior, we take a particle size of 8 mm and one layer as the base case

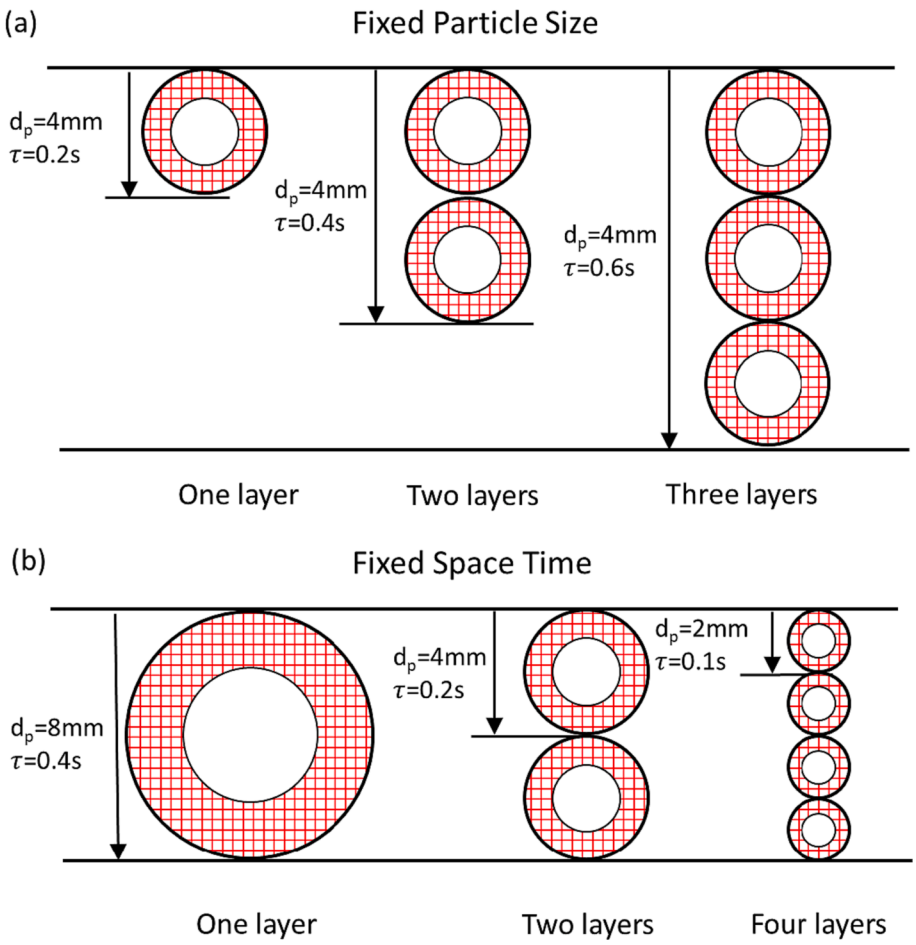

Fig. 7. Two packing strategies for multilayered beds with eggshell catalyst particles with (a) fixed particle size and varied space time and number of layers, and (b) fixed space time and varied particle diameter and number of layers.

and change the particle size and number of layers while keeping the space time constant. Fig. 10 shows the impact of particle size at a fixed space time on the ignited branch of the reactor. It is found that for case 3 (small particles), the extinction point moves to higher feed temperature which is consistent with the results as shown in Fig. 3. The oxygen conversion in the first case is only 80% due to the strong inter-phase mass transfer that occurs for larger particles. Instead of using one large particle, case 2 and case 3 use, respectively, a two-layer bed with 4 mm particles and a four-layer bed with 2 mm particles to reduce inter-phase mass transfer resistance, thereby increasing reactant conversion. As the number of layers increases and particle size decreases, oxygen conversion approaches 100% and ethane conversion increases from 14% to 18% while the ethylene selectivity remains nearly constant. Therefore, it is possible to use a multi-layered bed consisting of eggshell particles with a thin active layer to reach about 18% ethane conversion per pass and about 80% ethylene selectivity. Since the inter-phase mass and heat transfer times for the 2 mm particle are only about 8 ms, which is much smaller than the operating space time of 0.4 s, we could consider that the four-layer bed with 2 mm particles could reach the pseudo-homogeneous model limit (with the same volume of active catalyst). These calculations provide insights into designing shallow packed-bed reactors for ODHE that contain a few layers of eggshell catalyst particles.

5. Summary and discussion

One main contribution of this study is the elucidation of the ignition-extinction behavior of a single eggshell type catalyst particle (or a bed consisting of a single layer of particles) exposed to various ethane to oxygen ratios and feed temperatures. In this analysis, we used a six-step global kinetic model that has previously been validated using experimentally measured data over an MoVTeNbOx (M1) catalyst. In our view, the eggshell catalyst with an active layer thickness of about 0.2 mm is the most appropriate method for scale-up of the ODHE process as pore diffusional limitations become important (and reduce the ethylene selectivity) for any larger dimensions of the catalyst layer (at P = 1 bar). Further, any design that uses small particles and high flow rates may result in a high pressure drop, and hence may not be viable as a scale-up option. Our results indicate that it is possible to operate a multi-layered shallow-bed reactor autothermally using eggshell catalyst particles coated with a thin active layer (0.2 mm) at a space time of 0.4 s and a C_2H_6:O_2 feed ratio of 6. With finite size eggshell particles (2 to 4 mm), external mass transfer limitations can increase the ethane to oxygen ratio from 6 to approximately 30 as the gas mixture diffuses from the bulk gas phase to the ignited catalyst particle surface, resulting in increased ethylene selectivity for the specific ODHE kinetics under consideration in which undesired side reactions are more sensitive to O_2 pressure than desired dehydrogenation reactions. These mass transfer resistances, however, also limit ethane and oxygen conversions. Furthermore, the region of multiplicity is reduced for small catalyst particles where external mass transfer resistances are negligible. Therefore, it is important to identify the optimal reaction conditions (particle size, space time, active layer and so forth) to optimize the performance of eggshell catalyst particles in a manner that makes autothermal operation viable. Strong pore diffusion inside the particle consistently diminishes not only the region of multiplicity but also the ethylene selectivity. Employing an eggshell catalyst particle with a

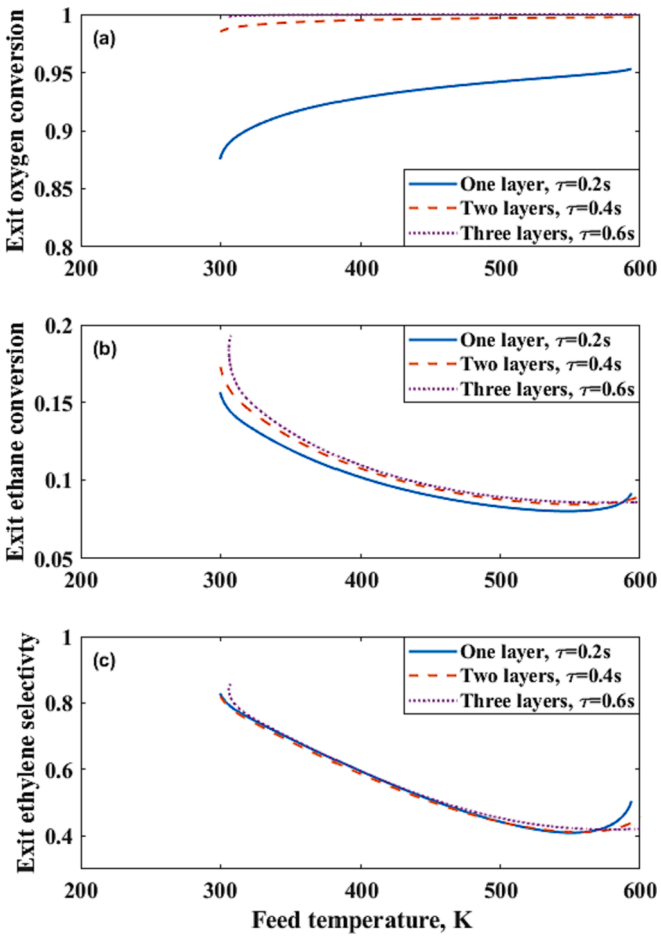

Fig. 8. Calculated exit (a) oxygen conversion, (b) ethane conversion, and (c) ethylene selectivity versus feed temperature for multilayered beds with eggshell particles in the ignited branch. Reaction conditions: $C_2H_6 : O_2 = 6$, $d_p = 4$ mm, $\xi_c = 0.2$ mm.

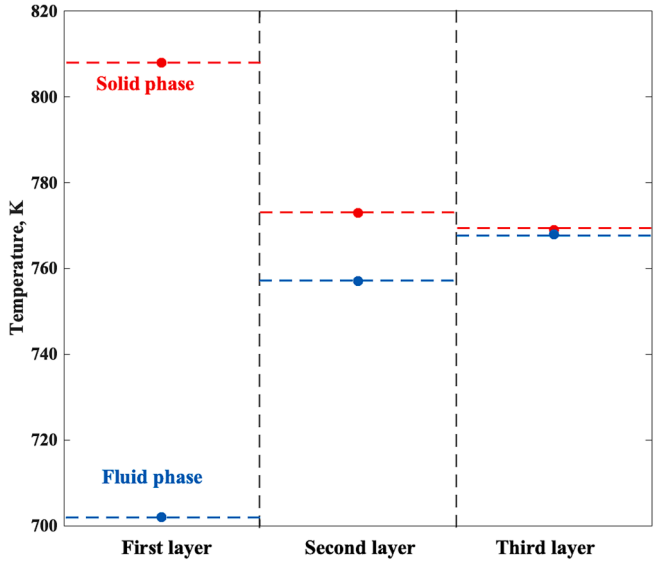

Fig. 9. Solid and fluid temperature in each layer corresponding to a feed temperature that is slightly to the right of the extinction point for a bed comprised of three layers of eggshell particles. Reaction conditions: P = 1 bar$C_2H_6 : O_2 = 6$, $d_p = 4$ mm, $\xi_c = 0.2$ mm.

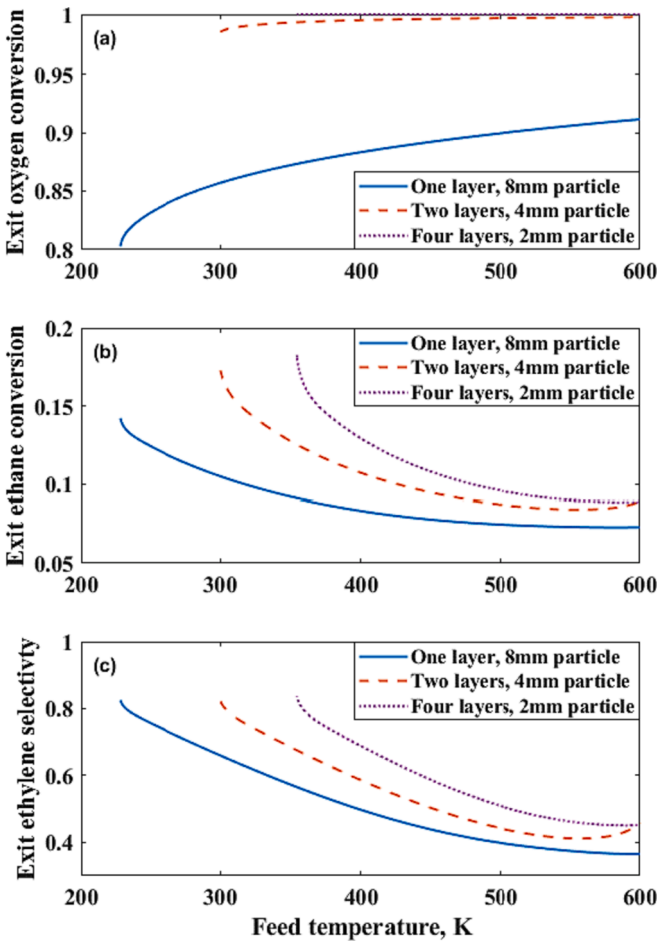

Fig. 10. Calculated exit (a) oxygen conversion, (b) ethane conversion, and (c) ethylene selectivity versus feed temperature for three different cases with a fixed space time of 0.4 s. Case 1: $d_p = 8$ mm, one layer, Case 2: $d_p = 4$ mm, two layers, Case 3: $d_p = 2$ mm, four layers. Reaction conditions: $C_2H_6 : O_2 = 6$, $\xi_c = 0.2$ mm.

suitable active catalyst layer thickness can help effectively avoid pore diffusional effects while still allowing for autothermal operation with near-ambient temperature feeds.

A second contribution of this work is the analysis of a multi-layered shallow-bed reactor with eggshell particles for scale-up of OHDE. We investigated the impact of packing strategies on the ignition and extinction behaviors. Specifically, we explored the impact of varying the space time and number of layers while keeping catalyst particle size fixed, and the effects of varying catalyst particle size and number of layers while keeping the space time fixed. In the first scenario, the location of the extinction point remains almost unchanged due to constant particle sizes. Oxygen is almost fully converted, and ethylene selectivity remains unchanged as the number of layers increases. Moreover, it is observed that the solid temperature decreases slightly, and the fluid temperature increases monotonically with an increase in the number of layers because the Lewis number (based on the diffusivity of the limiting reactant oxygen) is smaller than unity for the ODHE system under consideration. As is well known, when the Lewis number is less than 1, the heat removal rate from the particle is smaller than the mass transfer rate, and therefore the particle temperature can be higher than the adiabatic temperature rise. This is a unique phenomenon observed only in the ODHE system. In contrast, in oxidative coupling of methane (OCM), the system does not exhibit this behavior as the Lewis number is very close to unity or slightly higher. As for the case of fixed space time, smaller particle sizes always lead to a shrinking of the region

of multiplicity, and a shifting of the extinction point to higher feed temperatures. Using a bed with multiple layers and smaller catalyst particles could also help achieve complete oxygen conversion.

We now discuss some limitations and possible extensions of the results presented here. Firstly, our kinetic model is not comprehensive as it does not include products present in small concentrations such as acetic acid or acetaldehyde and their deep oxidation to CO or CO_2. However, a more detailed analysis using a kinetic model that includes these products is not expected to change the main conclusions of this work. Secondly, we only considered the steady-state behavior of the autothermal reactor. However, proper start-up to reach the operating point on the ignited branch is also an equally important aspect of reactor scale-up. The start-up process requires determining appropriate initial conditions and selecting the proper inlet reactant composition and temperature to maintain a constant bed temperature at the desired level until the system reaches steady state. This requires a detailed examination of the transient (dynamic) behavior of the reactor. Another limitation is that our analysis only accounts for the temperature gradient in the axial direction, and we do not consider radial variations (due to flow distribution or pattern formation). Detailed 2D or 3D models could be used to further analyze pattern formation and flow distributions. Another limitation of this work is that the model used here does not consider heat conduction (or backflow) between cells. It is known that including heat conduction in the solid makes the temperature profile more uniform and moves the extinction point to slightly lower feed temperatures or space times [20]. In addition, we ignored the variation of physical properties and any instability induced due to coupling between the species, energy, and momentum balances. Extension of these results to 3D models are topics of interest for future investigations.

Declaration of Competing Interest

The authors declare that they have no known competing financial interests or personal relationships that could have appeared to influence the work reported in this paper.

Data availability

Data will be made available on request.

Acknowledgements

The authors acknowledge funding from the National Science Foundation (Grant # CBET-2133174).

Appendix A. Supplementary data

Supplementary data to this article can be found online at https://doi.org/10.1016/j.cej.2023.145660.

References

[1] J.J.H.B. Sattler, J. Ruiz-Martinez, E. Santillan-Jimenez, B.M. Weckhuysen, Catalytic dehydrogenation of light alkanes on metals and metal oxides, Chem. Rev. 114 (2014) 10613–10653, https://doi.org/10.1021/cr5002436.
[2] M. Monai, M. Gambino, S. Wannakao, B.M. Weckhuysen, Propane to olefins tandem catalysis: A selective route towards light olefins production, Chem. Soc. Rev. 50 (2021) 11503–11529, https://doi.org/10.1039/d1cs00357g.
[3] S. Bilgen, İ. Sarıkaya, New horizon in energy: Shale gas, J. Nat. Gas Sci. Eng. 35 (2016) 637–645, https://doi.org/10.1016/j.jngse.2016.09.014.
[4] L. Ping, Y. Zhang, B. Wang, M. Fan, L. Ling, R. Zhang, Unraveling the surface state evolution of IrO_2 in ethane chemical looping oxidative dehydrogenation, ACS Catal. 13 (2) (2023) 1381–1399.
[5] J. Le Bars, A. Auroux, M. Forissier, J.C. Vedrine, Active sites of V_2O_5/γ-Al_2O_3 catalysts in the oxidative dehydrogenation of ethane, J. Catal. 162 (1996) 250–259, https://doi.org/10.1006/jcat.1996.0282.
[6] M.D. Argyle, K. Chen, A.T. Bell, E. Iglesia, Ethane oxidative dehydrogenation pathways on vanadium oxide catalysts, J. Phys. Chem. B 106 (2002) 5421–5427, https://doi.org/10.1021/jp0144552.
[7] E. Heracleous, A.A. Lemonidou, Ni-Me-O mixed metal oxides for the effective oxidative dehydrogenation of ethane to ethylene - Effect of promoting metal Me, J. Catal. 270 (2010) 67–75, https://doi.org/10.1016/j.jcat.2009.12.004.
[8] X. Zhao, M.D. Susman, J.D. Rimer, P. Bollini, Tuning selectivity in nickel oxide-catalyzed oxidative dehydrogenation of ethane through control over non-stoichiometric oxygen density, Catal. Sci. Technol. 11 (2021) 531–541, https://doi.org/10.1039/d0cy01732a.
[9] B. Solsona, J.M. López Nieto, P. Concepción, A. Dejoz, F. Ivars, M.I. Vázquez, Oxidative dehydrogenation of ethane over Ni-W-O mixed metal oxide catalysts, J. Catal. 280 (2011) 28–39, https://doi.org/10.1016/j.jcat.2011.02.010.
[10] A.M. Gaffney, O.M. Mason, Ethylene production via oxidative dehydrogenation of ethane using M1 catalyst, Catal. Today 285 (2017) 159–165, https://doi.org/10.1016/j.cattod.2017.01.020.
[11] Y.S. Yun, M. Lee, J. Sung, D. Yun, T.Y. Kim, H. Park, K.R. Lee, C.K. Song, Y. Kim, J. Lee, Y.J. Seo, I.K. Song, J. Yi, Promoting effect of cerium on MoVTeNb mixed oxide catalyst for oxidative dehydrogenation of ethane to ethylene, Appl. Catal. B Environ. 237 (2018) 554–562, https://doi.org/10.1016/j.apcatb.2018.06.025.
[12] E.V. Ishchenko, T.Y. Kardash, R.V. Gulyaev, A.V. Ishchenko, V.I. Sobolev, V. M. Bondareva, Effect of K and Bi doping on the M1 phase in MoVTeNbO catalysts for ethane oxidative conversion to ethylene, Appl. Catal. A 514 (2016) 1–13, https://doi.org/10.1016/j.apcata.2015.12.018.
[13] J. Chen, Z. Sun, P. Bollini, V. Balakotaiah, Scale-up analysis of the oxidative dehydrogenation of ethane over $MoVTeNbO_x$ catalysts in an autothermal reactor, Chem. Eng. Sci. 273 (2023), 118649, https://doi.org/10.1016/j.ces.2023.118649.
[14] V. Balakotaiah, Z. Sun, D.H. West, Autothermal reactor design for catalytic partial oxidations, Chem. Eng. J. 374 (2019) 1403–1419, https://doi.org/10.1016/j.cej.2019.05.155.
[15] A.G. Dietz, L.D. Schmidt, Conditions for HCN synthesis and catalyst activation over Pt-Rh gauzes, Appl. Catal. A 180 (1999) 287–298, https://doi.org/10.1016/s0926-860x(98)00350-0.
[16] S. Sarsani, D. West, W. Liang, V. Balakotaiah, Autothermal oxidative coupling of methane with ambient feed temperature, Chem. Eng. J. 328 (2017) 484–496, https://doi.org/10.1016/j.cej.2017.07.002.
[17] Z. Sun, D.H. West, P. Gautam, V. Balakotaiah, Scale-up analysis of autothermal operation of methane oxidative coupling with La_2O_3/CaO catalyst, AIChE J 66 (2020) 1–14, https://doi.org/10.1002/aic.16949.
[18] J. Chen, Z. Sun, V. Balakotaiah, P. Bollini, A global kinetic model for the oxidative dehydrogenation of ethane over mixed metal oxide catalysts at supra-ambient pressures, Chem. Eng. J. 445 (2022), 136605, https://doi.org/10.1016/j.cej.2022.136605.
[19] G.F. Froment, Kenneth B. Bischoff, J. De Wilde, Chemical Reactor Analysis and Design, 3rd edition, 2010. http://journal.um-surabaya.ac.id/index.php/JKM/article/view/2203.
[20] V. Balakotaiah, Z. Sun, T. Gu, D.H. West, Scaling relations for autothermal operation of catalytic reactors, Ind. Eng. Chem. Res. 60 (2021) 6565–6582, https://doi.org/10.1021/acs.iecr.0c05594.
[21] M. Shah, D. West, V. Balakotaiah, Bifurcation and stability analysis of temperature patterns in shallow-bed catalytic reactors, Chem. Eng. J. 446 (2022), 137146, https://doi.org/10.1016/j.cej.2022.137146.
[22] M. Shah, D. West, V. Balakotaiah, Analysis of temperature patterns in shallow-bed autothermal catalytic reactors, Chem. Eng. J. 437 (2022), 135027, https://doi.org/10.1016/j.cej.2022.135027.
[23] N. Wakao, T. Funazkri, Effect of fluid coefficients on particle-to-fluid mass transfer coefficients in packed beds: Correlation of sherwood numbers, Chem. Eng. Sci. 34 (1978) 1375–1384.
[24] N. Wakao, S. Kaguei, T. Funazkri, Effect of fluid dispersion coefficients on particle-to-fluid heat transfer coefficients in packed beds: Correlation of nusselt numbers, Chem. Eng. Sci. 34 (3) (1979) 325–336.
[25] E.N. Fuller, J.C. Giddings, A comparison of methods for predicting gaseous diffusion coefficients, J. Chromatogr. Sci. 3 (7) (1965) 222–227.
[26] M.M. Mezedur, M. Kaviany, W. Moore, Effect of pore structure, randomness and size on effective mass diffusivity, AIChE J. 48 (2002) 15–24, https://doi.org/10.1002/aic.690480104.
[27] M. Sadakane, K. Kodato, T. Kuranishi, Y. Nodasaka, K. Sugawara, N. Sakaguchi, T. Nagai, Y. Matsui, W. Ueda, Molybdenum-vanadium-based molecular sieves with microchannels of seven-membered rings of corner-sharing metal oxide octahedra, Angew. Chem. - Int. Ed. 47 (2008) 2493–2496, https://doi.org/10.1002/anie.200705448.
[28] T.T. Nguyen, M. Aouine, J.M.M. Millet, Optimizing the efficiency of MoVTeNbO catalysts for ethane oxidative dehydrogenation to ethylene, Catal. Commun. 21 (2012) 22–26, https://doi.org/10.1016/j.catcom.2012.01.026.
[29] L. Annamalai, Y. Liu, S. Ezenwa, Y. Dang, S.L. Suib, P. Deshlahra, Influence of tight confinement on selective oxidative dehydrogenation of ethane on MoVTeNb mixed oxides, ACS Catal. 8 (2018) 7051–7067, https://doi.org/10.1021/acscatal.8b01586.
[30] L. Annamalai, S. Ezenwa, Y. Dang, H. Tan, S.L. Suib, P. Deshlahra, Comparison of structural and catalytic properties of monometallic Mo and V oxides and M1 phase mixed oxides for oxidative dehydrogenation, Catal. Today 368 (2021) 28–45, https://doi.org/10.1016/j.cattod.2020.04.046.
[31] S. Matar, L.F. Hatch, Chemistry of petrochemical processes, Second edi, Elsevier, 2001.
[32] E. López, E. Heracleous, A.A. Lemonidou, D.O. Borio, Study of a multitubular fixed-bed reactor for ethylene production via ethane oxidative dehydrogenation, Chem. Eng. J. 145 (2008) 308–315, https://doi.org/10.1016/j.cej.2008.08.029.
[33] G. Che-Galicia, R.S. Ruiz-Martínez, F. López-Isunza, C.O. Castillo-Araiza, Modeling of oxidative dehydrogenation of ethane to ethylene on a $MoVTeNbO/TiO_2$ catalyst

in an industrial-scale packed bed catalytic reactor, Chem. Eng. J. 280 (2015) 682–694, https://doi.org/10.1016/j.cej.2015.05.128.
[34] K. Ramanathan, V. Balakotaiah, D.H. West, Light-off criterion and transient analysis of catalytic monoliths, Chem. Eng. Sci. 58 (2003) 1381–1405, https://doi.org/10.1016/S0009-2509(02)00679-6.
[35] S.R. Gundlapally, V. Balakotaiah, Heat and mass transfer correlations and bifurcation analysis of catalytic monoliths with developing flows, Chem. Eng. Sci. 66 (2011) 1879–1892, https://doi.org/10.1016/j.ces.2011.01.045.

Shallow-Bed Reactor Design for the Autothermal Oxidative Dehydrogenation of Ethane over $MoVTeNbO_x$ Catalysts

Jiakang Chen, Praveen Bollini*, Vemuri Balakotaiah*

William A. Brookshire Department of Chemical & Biomolecular Engineering,

University of Houston, Houston, TX 77204, USA

*Corresponding authors: ppbollini@uh.edu, bala@uh.edu

Supplementary Information

Contents

S1. Rate expressions

Table S1 lists the rate expressions constituting the proposed global kinetic model used to describe ethane oxidation rate data over the $MoVTeNbO_x$ catalyst under consideration. The model shows that the side reactions have a higher total pressure dependency than the desired dehydrogenation reaction.

Table S1. Global kinetic model rate expressions used to describe ethane oxidation rate data over $MoVTeNbO_x$.

Reaction steps	Rate expression
$R1$: $C_2H_6 + 0.5O_2 \rightarrow C_2H_4 + H_2O$	$\mathrm{r}_1 = \dfrac{k_1' P_{\mathrm{C_2H_6}}}{\left(1 + \sqrt{\dfrac{k_1' P_{\mathrm{C_2H_6}}}{2\mathrm{k_o} P_{o_2}}}\right)^2}$
$R2$: $C_2H_6 + 2.5O_2 \rightarrow 2CO + 3H_2O$	$r_2 = k_2 P_{\mathrm{C_2H_6}} {P_{o_2}}^{0.5}$
$R3$: $C_2H_6 + 3.5O_2 \rightarrow 2CO_2 + 3H_2O$	$r_3 = k_3 P_{\mathrm{C_2H_6}} {P_{o_2}}^{0.5}$
$R4$: $C_2H_4 + 2O_2 \rightarrow 2CO + 2H_2O$	$r_4 = k_4 P_{\mathrm{C_2H_4}} {P_{o_2}}^{0.5}$
$R5$: $C_2H_4 + 3O_2 \rightarrow 2CO_2 + 2H_2O$	$r_5 = k_5 P_{\mathrm{C_2H_4}} {P_{o_2}}^{0.5}$
$R6$: $CO + 0.5O_2 \rightarrow CO_2$	$r_6 = k_6 P_{CO} {P_{o_2}}^{0.5}$

S2. Kinetic parameters

Table S2 lists pre-exponential factors and activation energies for each step with a 90% confidence interval. We use these kinetic parameters to perform scale-up analysis of the ODHE process.

Table S2. Estimated pre-exponential factors and apparent activation energies with 90% confidence intervals

Reaction steps	$k_{0,i}$ (mol/s/g_{cat}/kPa^m)	$E_{a,j}$ (kJ/mol)
1	3.59 ± 0.57	89.4 ± 3.7
	490.4 ± 430.8	101.6 ± 5.1
2	39.37	138.4
3	17.59	130.7
4	7.31 ± 4.28	120.8 ± 4.4
5	3.69 ± 2.77	122.1 ± 9.3
6	7.36E-5 ± 3.96E-5	52.8 ± 3.2

The rates are expressed as mol/g cat/s and can be converted to moles/cm^3/s by multiplying the catalyst bulk density (ρ_c=1.60 g/cm^3). The rates can be converted to units of s^{-1} by dividing the rates having units of moles/cm^3/s by the total molar concentration in gas phase having units of moles/cm^3.

S3. Characteristic inter-phase mass and heat transfer timescales

Table S3 lists the inter-phase mass and heat transfer times at two different temperatures and particle sizes with fixed linear velocity. As expected, mass and heat transfer times increase with particle size but decrease with temperature.

Table S3. Calculated mass and heat transfer times at different temperature and particle size, linear velocity is 0.04 m/s.

Temperature (K)	Particle size (mm)	τ_{mi} at 1 bar (ms)	τ_{hi} at 1 bar (ms)	τ_{mi} at 5 bar (ms)	τ_{hi} at 5 bar (ms)
650	1	1.9	2.3	6.32	7.32
	2	6.6	7.7	19.6	22.6
	4	21.7	25.2	58.4	66.9
	8	68	78	168	192
750	1	1.6	1.8	5.4	6.0
	2	5.5	6.2	16.8	18.7
	4	18	21	50	56
	8	58	65	148	163

S4. Impact of feed ratio

Figure S1 shows the exit particle temperature, reactants conversion and ethylene selectivity as a function of feed temperature for different ethane to oxygen feed ratios. It is found that the region of multiplicity increases with decreasing feed ratio. Lower feed ratio yields higher ethane conversion but also lower ethylene selectivity.

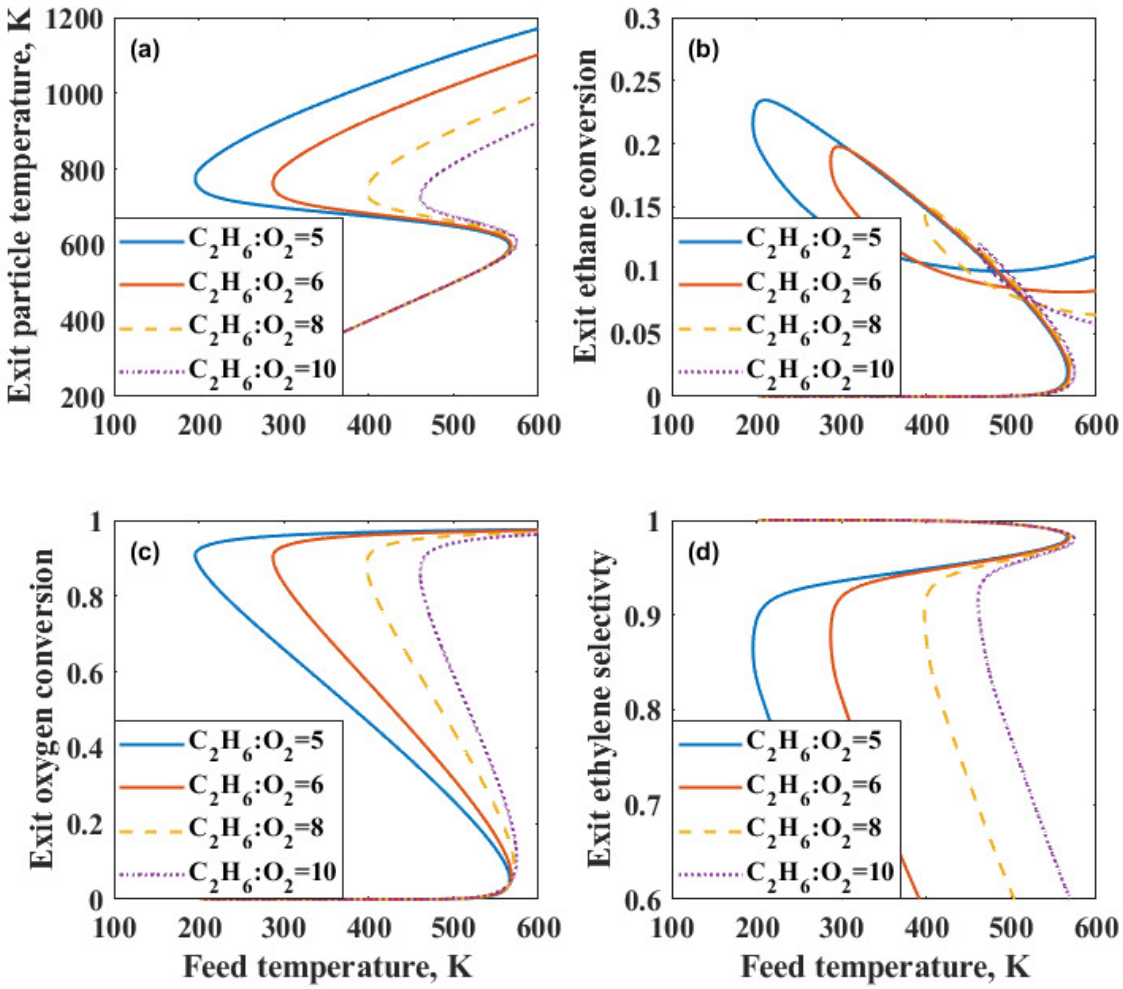

Figure S1. Computed bifurcation diagrams of exit (a) particle temperature, (b) ethane conversion, (c) oxygen conversion, and (d) ethylene selectivity versus feed temperature at different feed ratio. Reaction conditions: τ=0.4s, d_p=4mm, ξ_c=0.1d_p, P=1bar.

S5. Impact of active layer depth

Figure S2 shows the exit particle temperature, reactants conversion and ethylene selectivity as a function of feed temperature for different active layer lengths. As the active layer length increases from 0.2 mm to 0.4 mm, both ignition and extinction points move to lower feed temperature. However, the region of multiplicity remains unchanged as the active layer length increases from 0.6 mm to 0.8 mm. That is because oxygen is almost consumed at the outermost part of the active layer and no additional reaction occurs with further increases in the active layer length.

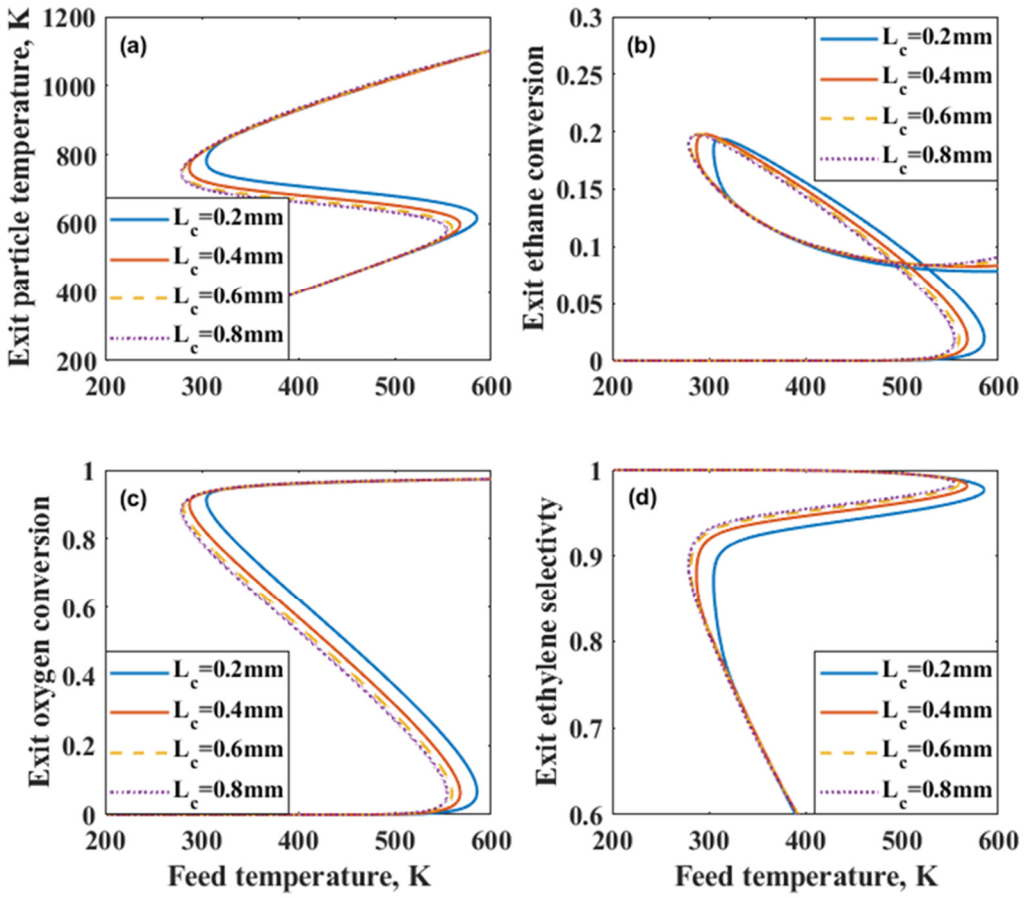

Figure S2. Computed bifurcation diagrams of exit (a) particle temperature, (b) ethane conversion, (c) oxygen conversion, and (d) ethylene selectivity versus feed temperature at different active layer length. Reaction conditions: C_2H_6:O_2=6, τ=0.4s, d_p=4mm, P=1bar.

S6. Impact of operating pressure

Figure S3 and Figure S4 show the dependence of exit particle temperature, reactant conversion, and ethylene selectivity on feed temperature under varying total pressure conditions for two scenarios: fixed linear velocity and fixed mass velocity.

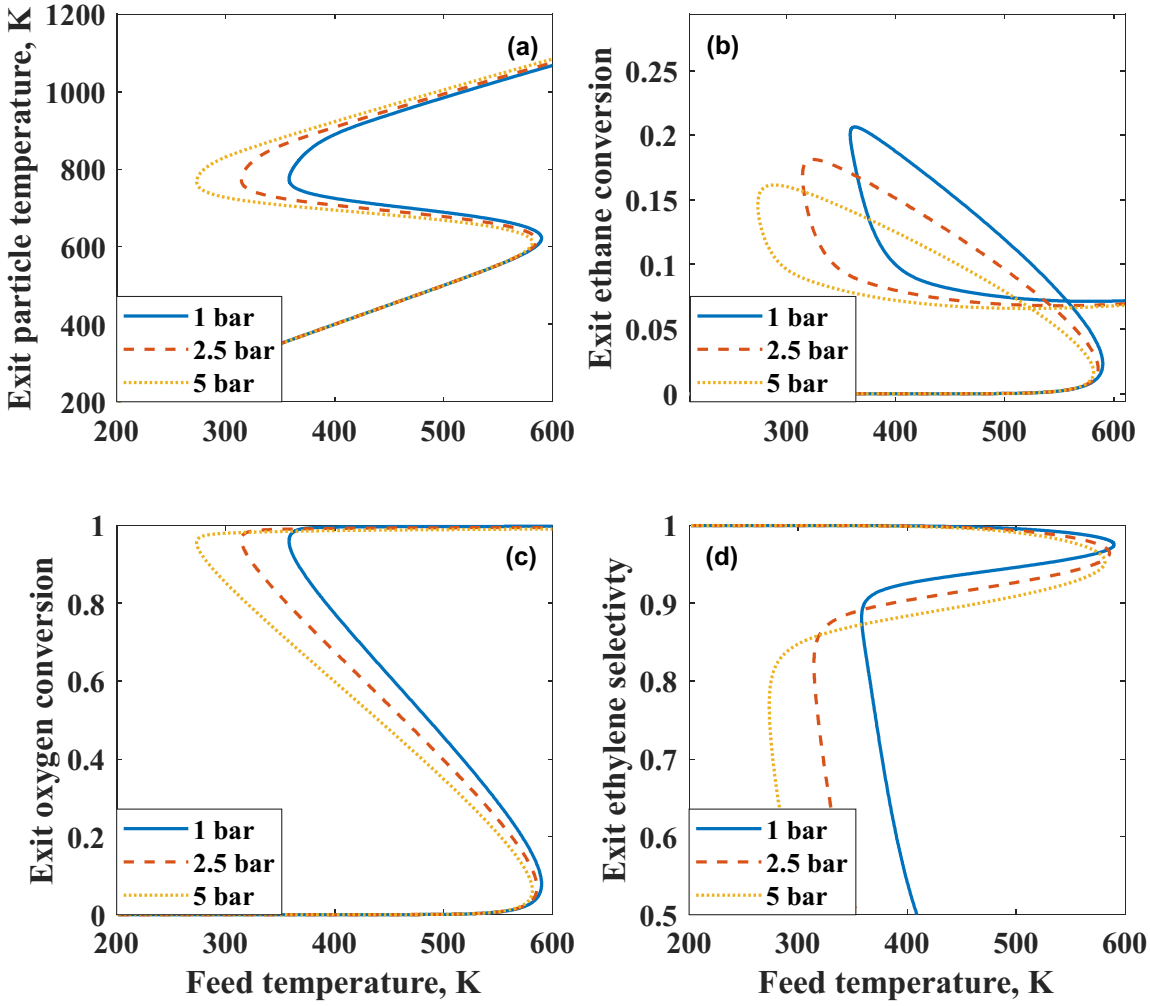

Figure S3. Calculated exit (a) particle temperature, (b) ethane conversion, (c) oxygen conversion, and (d) ethylene selectivity versus feed temperature for different total pressures with fixed linear velocity. Reaction conditions: C_2H_6: O_2=6, d_p=1mm, ξ_c=0.05mm, τ=0.4s

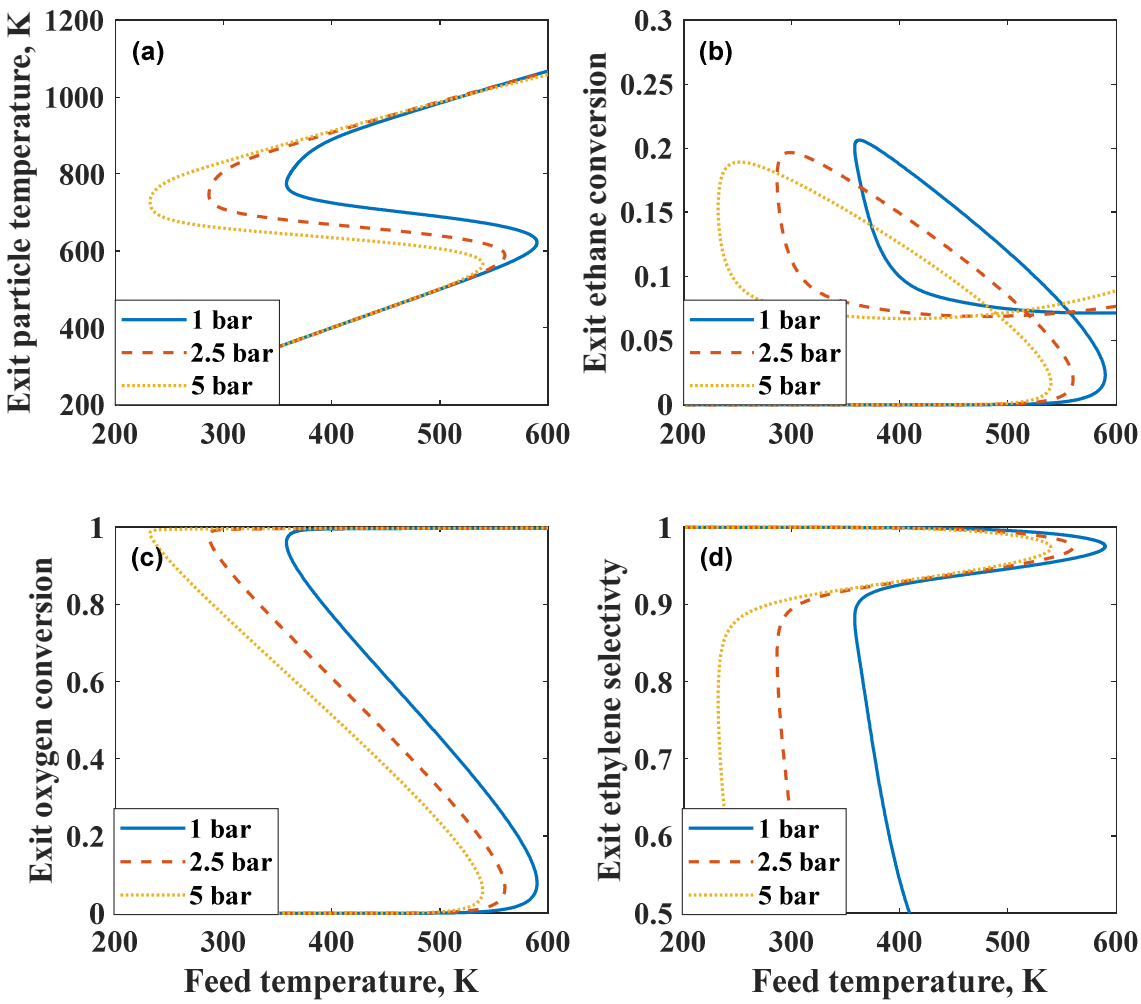

Figure S4. Calculated exit (a) particle temperature, (b) ethane conversion, (c) oxygen conversion, and (d) ethylene selectivity versus feed temperature for different total pressures with fixed mass velocity. Reaction conditions: C_2H_6: O_2=6, d_p=1mm, ξ_c=0.05mm, τ=0.4-2.0s

S7. Impact of reactants dilution

Figure S5 illustrates the bifurcation diagram obtained at a feed ratio of 4, a particle diameter of 2 mm, and a space time of 3 s with 50% methane dilution.

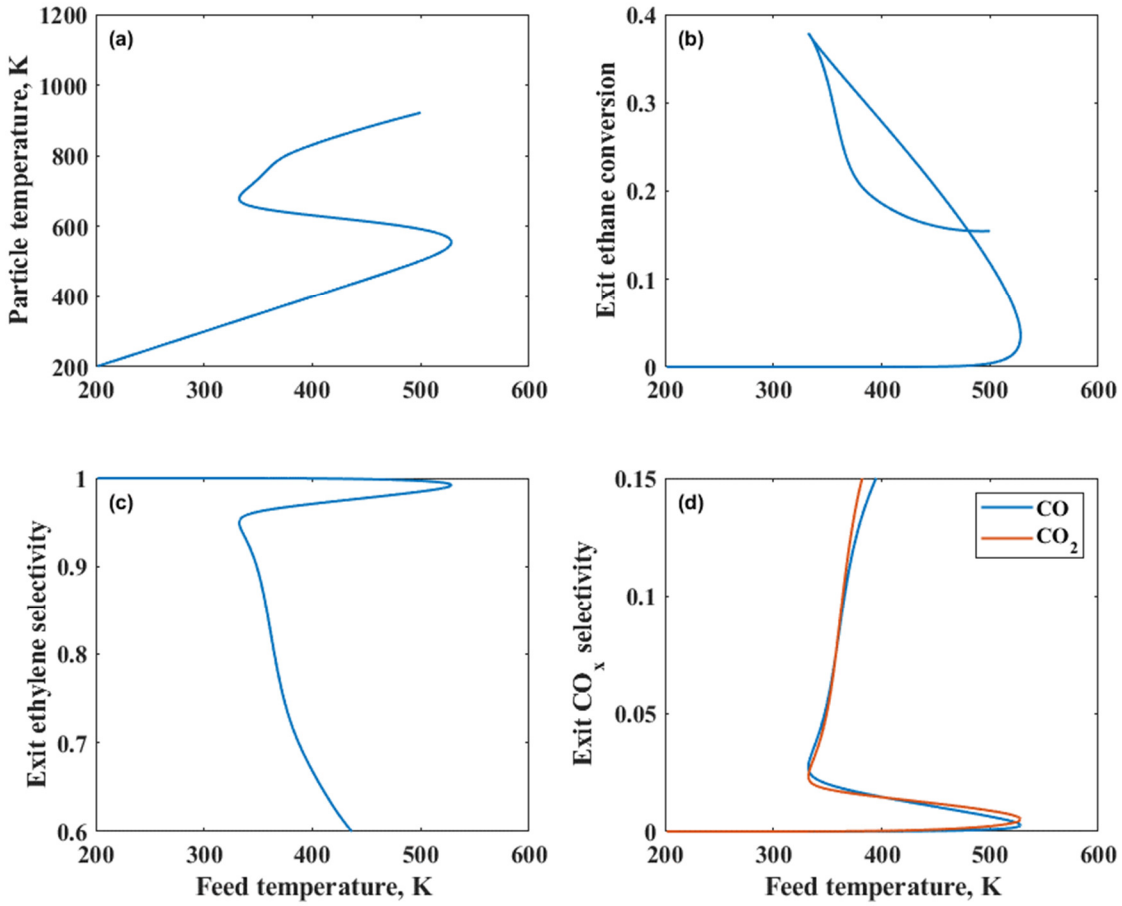

Figure S5. Calculated exit (a) particle temperature, (b) ethane conversion, (c) oxygen conversion, and (d) ethylene selectivity versus feed temperature with 50% methane dilution. Reaction conditions: C_2H_6: O_2=4, d_p=2mm, ξ_c=0.2mm, τ=3.0s, P=1bar.

S8. Bifurcation diagram for multilayered beds

Figure S6 shows the exit solid and fluid temperature as a function of feed temperature for a three-layer bed with eggshell particles. It is found that solid temperature decreases with increasing number of layers while the fluid temperature monotonically increases.

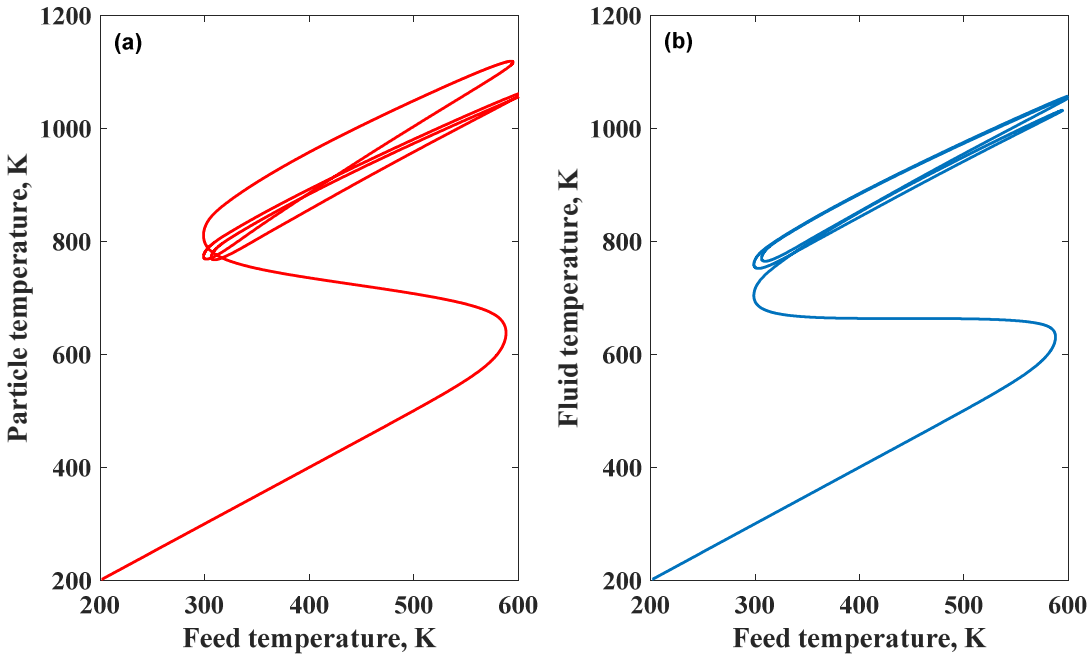

Figure S6. Bifurcation diagram of exit (a) particle temperature (b) fluid temperature versus feed temperature for a bed composing three layers of eggshell particles. Reaction conditions: C_2H_6: O_2=6, d_p=4mm, ξ_c=0.2mm.

S9. Pressure drop in shallow-bed reactors

This section presents an analysis of the pressure drop in a multilayered bed containing 3 or 4 catalyst particle layers. The calculation of pressure gradient employs the Ergun Equation [1], which is expressed as follows:

$$\frac{dP}{dL} = -\left(150\frac{\mu_f u(1-\epsilon)^2}{d_P^2\epsilon^3} + 1.75\frac{\rho_f u^2(1-\varepsilon)}{d_p\varepsilon^3}\right), \quad (9a)$$

where dP is the pressure drop in a differential length dL of the reactor, μ_f is the viscosity of reaction mixture passing through the bed, u is the linear velocity, ϵ is the bed porosity, ρ_f is the fluid density, d_p is the catalyst particle diameter. Since high ethane to oxygen feed ratio is used in most of our calculations, we use the physical properties of ethane to represent the gas density and viscosity in the pressure drop calculations. Four particle layers, each with a diameter of 4 mm, are selected to calculate the base case for pressure drop. Consequently, the total length of the catalyst bed is about 16 mm. The bed porosity is calculated as shown below [2]:

$$\varepsilon = 1 - (\frac{\rho_b}{\rho_s}), \quad (9b)$$

where ρ_b is the catalyst bulk density and ρ_s is the sold catalyst density. The porosity of the bed is estimated to be approximately 0.36.

Table S4 presents the pressure drops for the multilayered bed, which range from 0.00029 to 0.0037 kPa as the linear velocity increases from 0.01 to 0.08 m/s at pressure of 5 bar. The pressure drop is even smaller at 1 bar. These results suggest that the pressure drop along the bed can be considered negligible.

Table S4. Pressure drops as a function of different linear velocities for multilayer bed.

Linear velocity (m/s)	0.01	0.02	0.04	0.08
Pressure drop at 1 bar (kPa)	0.00026	0.00054	0.0011	0.0024
Pressure drop at 5 bar (kPa)	0.00029	0.00063	0.0014	0.0037

References:

[1] N. Varde, H.S. Fogler, Elements of chemical reaction engineering, fifth ed., Pearson Education, Inc., IN, 2006.

[2] A.S. Pushnov, Calculation of average bed porosity, Chem. Pet. Eng. 42 (2006) 14–17. https://doi.org/10.1007/s10556-006-0045-x.